arXiv:2409.02554v1 [astro-ph.SR] 4 Sep 2024

DH type II radio bursts during solar cycles 23-25: Origin and association with solar eruptive events

Bhuwan Joshi[1], Binal D. Patel[1], Kyung-Suk Cho[2], and Rok-Soon Kim[2]

[1]Udaipur Solar Observatory, Physical Research Laboratory, Udaipur 313001, India
email: bhuwan@prl.res.in
[2]Space Science Division, Korea Astronomy and Space Science Institute, Daejeon 34055, Republic of Korea

Abstract. We analyses occurrence of DH type II solar radio bursts spanning over solar cycles 23-25 during which a total of 590 DH type II bursts are reported with confirmed 568 and 462 cases of associated CME and flares, respectively. We find short-term yet important differences in DH type II activity when the data is examined in terms of event counts and their durations, e.g., temporal shift in the peak activity during cycle 24 and variation in the growth rate of the activity level during cycle 25. For an in-depth exploration, DH type II bursts are classified in 3 categories based on their end-frequencies: Low-, Medium-, and High- Frequency Groups (LFG, MFG, and HFG, respectively). The HFG category is the most populous ($\approx$47%) while the LFG category occupy about a quarter of the events ($\approx$24%). The LFG events show a clear inclination toward fastest CMEs and X-class flares with a quarter of events exhibiting end frequency below 50 MHz.

Keywords. Coronal mass ejections, solar radio bursts, type II bursts, solar cycle

1. Introduction

It is well recognized that the powerful CMEs generate shocks in the coronal and interplanetary medium. In radio dynamic spectrum, these shocks are identified as type II bursts. Depending on the energetics of CMEs, the type II bursts are observed in metric (m;30 MHz $\leq$ f $\leq$ 300 MHz), decametric–hectometric (DH; 300 kHz $\leq$ f $\leq$ 30 MHz), and kilometric (km; 30 kHz $\leq$ f $\leq$ 300 kHz) wavelength domains. The extension or origin of type II radio bursts in the DH domain implies the cases of stronger MHD shocks propagating from the inner corona and entering the interplanetary (IP) medium (Gopalswamy et al. 2001, 2005). Hence the study of shocks in DH domain, together with their associated CME-flare events, becomes extremely important to infer not only the propagation characteristics of CMEs but also to develop their forecasting tools (Reiner et al. 2007; Joshi et al. 2018; Syed Ibrahim et al. 2019). Contextually, the CME associated with type II radio bursts in metric and/or DH wavelength domain are termed as radio loud CMEs (Michalek et al. 2007; Gopalswamy et al. 2008).

Table 1. Occurrence of DH type II radio bursts from January 1996 to June 2023, covering solar cycles 23-25, along with the identified solar events, i.e., CMEs and flares, occurred in association with the reported bursts.

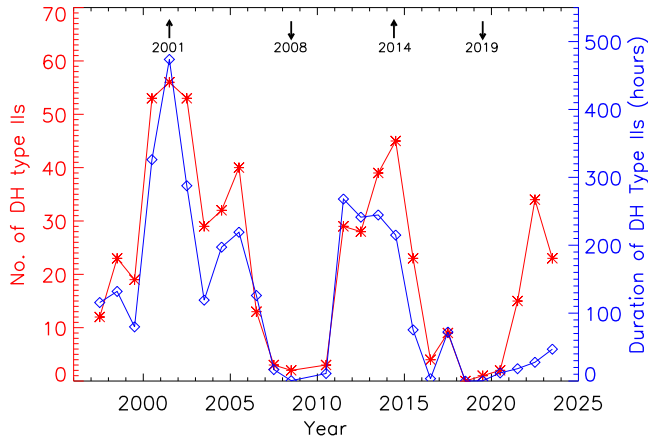| Solar Cycle	No. of Events		
	DH type II	Identified solar events	
	(% out of total)	CME	Flare
23	335 (57%)	320	275
24	180 (30%)	173	127
25	75 (13%)	75	60
23+24+25	590	568	462

Figure 1. Annual occurrence of DH type II radio bursts from January 1996 to June 2023, covering solar cycle 21, 22, and rising phase of cycle 23 in terms of counts and cumulative durations over a year. Up and down arrows represent the maximum and minimum years of solar cycles.

In this paper, we present a statistical study of DH type II bursts occurred during solar cycles 23, 24, and 25. For the present analysis, we have obtained data from the following sources: (1) Wind/WAVES Type-II Burst Catalogue (`https://cdaw.gsfc.nasa.gov/CME_list/radio/waves_type2.html`), (2) Solar and Heliospheric Observatory (SOHO) Large Angle and Spectroscopic Coronagraph (LASCO) CME Catalogue(`https://cdaw.gsfc.nasa.gov/CME_list/`). This work highlights the importance of analysing DH type II bursts in terms of their end frequencies (Patel et al. 2021, 2022). Notably, the end frequencies of these IP bursts directly relate to the heliocentric distance up to which a shock can survive and, therefore, have implications in exploring the energetics and propagation characteristics of CMEs.

2. Occurrence and frequency-dependent characteristics

2.1. *DH type II bursts during cycles 23-25*

A comparison of occurrence of DH type II radio bursts during solar cycles 23 (January 1996–December 2008), 24 (January 2009–Dec 2017, and 25 (January 2018–June 2023) shows that cycle 23 produced about twice number of events than cycle 24 (Table 1). The solar cycle 25 is still running, however, in the beginning phase of ≈ 5 years, considered here, it has exhibited a deficit in DH type II activity compared to the previous two cycles along with a slow rise. To understand the activity level of DH type II radio bursts with the evolution of solar cycles, we characterize the type II activity in terms of their total yearly counts and cumulative durations (Figure 1). Both indicators reflect an obvious cyclic behaviour of ≈ 11 years with some noteworthy differences: the maximum activity period for the two parameters differs for cycle 24, and type II event counts show a steep growth during 2021-2023 while the cumulative durations indicates a slow and gradual rise. To have a clear understanding of the observed DH type II events in terms of the frequency at which the bursts originated or first detected, we present a histogram of the starting frequencies in Figure 2. Here we clearly notice that the histogram bars representing the limiting frequency range of Wind/WAVES (13–14 MHz) and SWAVES (15–16 MHz) populate 45% and 12% events, respectively. From this statistics, it is clear that a sizeable population of DH type II events exist as an extension of type II emission starting at metric frequencies.
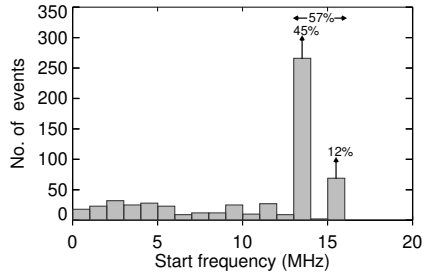
Figure 2. Distribution of start frequencies of DH type II radio bursts for a total of 590 events of our data set.
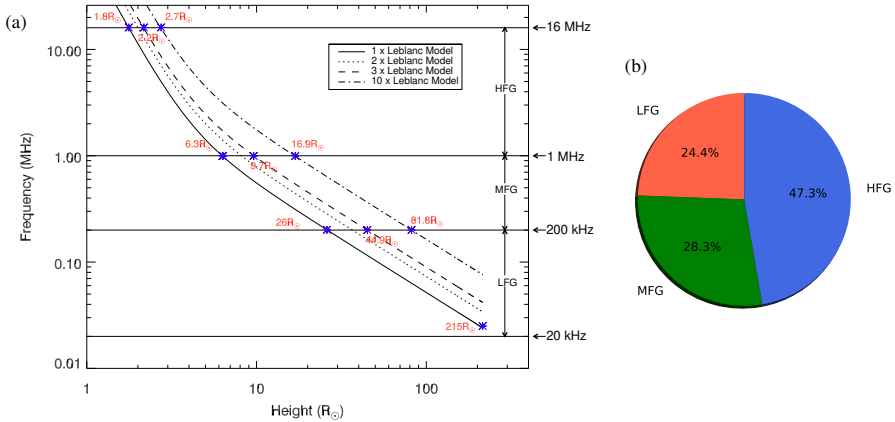

Figure 3. (a) Variation of heliocentric burst height ($R_\odot$) with plasma frequency estimated from Leblanc electron density model. (b) Pie chart showing the fraction of LFG (red), MFG (blue), and HFG (green) DH type II radio bursts occurred during cycles 23-25.

2.2. *Frequency-dependent categories and their characteristics*

The characteristics feature of type II burst is slow frequency drift toward lower frequencies which is physically attributed to the burst driver moving outward from the solar atmosphere to larger heliocentric distances with ever decreasing electron densities. This frequency–height relationship of the type II burst is illustrated using the atmospheric density model of Leblanc et al. (1998) in Figure 3. Contextually, we note that the height estimations from the atmospheric density model provide a "coarse" estimation only as the density of the medium, through which shock is propagating, evolves with the spatially and temporally varying coronal and interplanetary conditions. Thus, rationally, we consider a multiplier (or suitable "fold") to the basic atmospheric density model.

Table 2. Occurrence of DH type II events during Solar Cycles 23, 24, and 25 for LHG, MFG, and HFG categories.

Solar Cycle	Number of events			
	LFG	MFG	HFG	Total
	$f \leq 200$ kHz	200 kHz $< f \leq 1$ MHz	1 MHz $< f \leq 16$ MHz	
23	81(24%)	96 (29%)	158 (47%)	335 (57%)
24	57 (32%)	55 (30%)	68 (38%)	180 (31%)
25	6 (8%)	16 (21%)	53 (71%)	75 (13%)
23+24+25	144 (24.4%)	167 (28.3%)	279 (47.3%)	590

In Figure 3a, we draw frequency-height relation for 1-, 2-, 3-, and 10-fold Leblanc models to incorporate density variations of upto an order. The frequency–height relationship suggests that
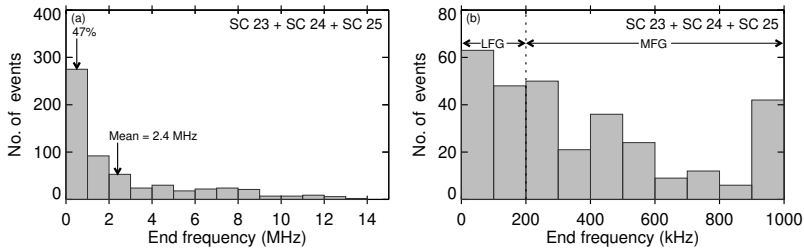
Figure 4. (a) Distribution of DH type II radio bursts in terms of their end frequencies. (b) Distribution of end frequencies exclusively for LFG and MFG events.

the observing window of 16 MHz–20 kHz essentially represents a large heliocentric distance from $\approx 2R_\odot$ to 1 AU. Therefore, to explore the characteristic of DH type II radio bursts and associated solar eruptive events, we divide this vast frequency range into three groups: Low-Frequency Group (LFG; 20 kHz $\leq$ f $\leq$ 200 kHz), Medium-Frequency Group (MFG; 200 kHz $\leq$ f $\leq$ 1 MHz), and High Frequency Group (HFG; 1 MHz $\leq$ f $\leq$ 16 MH. Figure 3a readily shows that our end-frequency classification essentially provides a quantitative estimation on the distance up to which a shock can survive. We further note that HFG and MFG events represent shocks terminating within the lower and upper coronal heights (9.7$R_\odot$ and 44.9$R_\odot$, as per three-fold Leblanc model), respectively. On the other hand, the events under LFG group represent shock travelling in the interplanetary medium (beyond $\approx 45R_\odot$).

In Table 2, we list the counts for LFG, MFG, and HFG events for solar cycle 23, 24, and 25. The same has been pictorially shown in a pie chart in Figure 3b. In Figure 4a, we present the histogram of ending frequency for DH type II events which reveal 49% of events to lie below 1 MHz frequency bin. We further show the distribution of ending frequencies from 1 MHz down to 20 KHz in Figure 4b to explore the occurrence of LFG and MFG events exclusively. In Table 3, we specifically give number of type II bursts that end beyond 50 MHz as this frequency roughly corresponds to heliocentric distance of 0.5 AU (see Figure 3a); We find cycle 24 to be highly deficient in comparison to cycle 23 (12% versus 37%) while rise phase of cycle 25 completes lacks such events.

Table 3. Occurrence of DH type II events having end frequency <50 kHz.

Solar Cycle	No. of Events (total events)	%
23	30 (81)	37%
24	7 (57)	12%
25	0 (6)	0
23+24+25	37 (144)	26

3. Association with CMEs and flares

In Figure 5, we present the distribution of linear speed of CMEs within LASCO field-of-view associated with DH type II radio bursts for HFG, MFG, and LFG categories. The histograms clearly reveal a larger difference of ≈ 570 km s^{-1} between the mean CME speeds for two limiting cases i.e., LFG and HFG categories. Further, as expected, the mean speed for MFG events lies between the LFG and HFG classes. To investigate whether the CME speeds for HFG, MFG, and LFG categories belong to the same distribution or not (i.e., if the difference in mean speeds of CMEs for the three successive categories is statistically significant), we perform the two-sample Kolmogorov–Smirnov test ((K-S test; Press et al. 1992) and the results of the test is presented in Table 4. The two-sample K-S test suggests that the difference
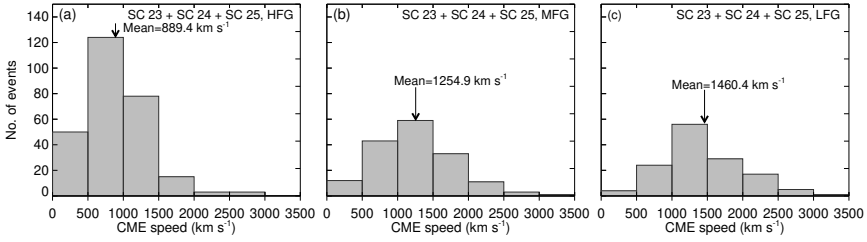
Figure 5. Histogram showing the distribution of linear speed of CMEs (within LASCO field-of-view) for events of HFG (panel a), MFG (panel b), and LFG (panel c) categories.
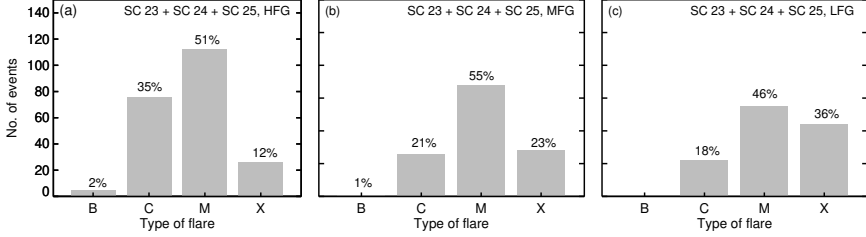

Figure 6. Histograms showing the distribution of flare counts of GOES classes (B, C, M, and X) associated with DH-type II radio bursts of HFG (panel a), MFG (panel b), and LFG (panel c) categories.

in the mean speed of CMEs between the events of three categories of DH type II radio bursts is statistically highly significant.

In Figure 6, we present the histogram showing the association of flares of different GOES classes (viz B, C, M, and X) with DH type II radio bursts. We find that the highest number of events are associated with the M class flares ($\approx$55%) for all the categories. We further find that the fraction of occurrence of X-class flares becomes almost double as we go from HFG to LFG categories (12, 23, and 36%, respectively).

Table 4. The results of the two-sample K-S test assessing the observed difference between mean CME speeds of HFG, MFG, and LFG categories. N_1 and N_2 represent the number of events for respective categories. The K-S test statistics and probability are denoted by D and P.

Category	ΔV (km s^{-1})	Sample Size N_1	N_2	D	P
$\Delta V_{MFG-HFG}$	365	162	273	0.33	2.5×10^{-10}
$\Delta V_{LFG-MFG}$	206	136	162	0.205	0.0032
$\Delta V_{LFG-HFG}$	571	136	273	0.515	5.7×10^{-22}

4. Conclusions

The present study make a detailed survey of DH type II radio bursts occurred during solar cycles 23-25 involving a total of 590 DH type II bursts from January 1996 to June 2023, with confirmed 568 and 462 cases of associated CME and flares, respectively. In the following, we summarize the main results of the paper:

(1) The occurrence rate of DH type bursts follow a periodic behaviour with the phases of solar cycle. However, subtle but important differences are seen when the data is examined in terms of event counts and event durations. This result has important implication in understanding the origin of solar activity and its coronal and heliospheric consequence.

(2) Our approach is to classify radio loud CMEs based on the end-frequencies of the corresponding DH type II radio bursts. Accordingly, three categories of CMEs have been considered viz. Low-Frequency Group (LFG; 20 kHz $\leq$ f $\leq$ 200 kHz), Medium-Frequency Group (MFG; 200 kHz $\leq$ f $\leq$ 1 MHz), and High Frequency Group (HFG; 1 MHz $\leq$ f $\leq$ 16 MH. This end-frequency classification plausibly describes the heliocentric distance up to which a shock can survive.

(3) The HFG category is the most populous, occupying almost half of the events of the entire sample ($\approx$47%). The LFG category (f $\leq$ 200 kHz), most important for space weather perspective, occupy a quarter of the events ($\approx$24%).

(4) Within the LFG class, $\approx$25% events exhibiting end frequency below 50 MHz, are of special interest as this frequency corresponds to a heliocentric distance of $\approx$0.5 AU. Notably, cycle 24 drastically lacks such events in comparison to cycle 23 (12% versus 37%). In cycle 25, we could not find any events of this category within the observing period (January 2018–June2023).

(5) The LFG events show a clear inclination toward fastest CMEs and largest X-class flares.

In summary, the present study provides us insights about the statistical properties of DH type II radio bursts during cycles 23-25 but also widens our understanding about the conditions related to their origin in the near-Sun region and survival in the corona and interplanetary medium. Our results indicate that the three-element classification of radio loud CMEs – HFG, MFG, and LFG – has important implications. In particular, the HFG events imply propagation of the shock inside the complex magnetic environment and within faster solar wind condition of the low corona, whereas, the events of LFG category, representing the shock travelling from the corona to the interplanetary medium, are rather intriguing for understanding the space weather phenomena.

References

Gopalswamy, N., Aguilar-Rodriguez, E., Yashiro, S., et al. 2005, Journal of Geophysical Research (Space Physics), 110, A12S07, doi: 10.1029/2005JA011158

Gopalswamy, N., Yashiro, S., Kaiser, M. L., Howard, R. A., & Bougeret, J. L. 2001, *JGR*, 106, 29219, doi: 10.1029/2001JA000234

Gopalswamy, N., Yashiro, S., Xie, H., et al. 2008, *ApJ*, 674, 560, doi: 10.1086/524765

Joshi, B., Ibrahim, M. S., Shanmugaraju, A., & Chakrabarty, D. 2018, *SoPh*, 293, 107, doi: 10.1007/s11207-018-1325-2

Leblanc, Y., Dulk, G. A., & Bougeret, J.-L. 1998, *SoPh*, 183, 165, doi: 10.1023/A:1005049730506

Michalek, G., Gopalswamy, N., & Xie, H. 2007, *SoPh*, 246, 409, doi: 10.1007/s11207-007-9062-y

Patel, B. D., Joshi, B., Cho, K.-S., & Kim, R.-S. 2021, *SoPh*, 296, 142, doi: 10.1007/s11207-021-01890-6

Patel, B. D., Joshi, B., Cho, K.-S., Kim, R.-S., & Moon, Y.-J. 2022, *SoPh*, 297, 139, doi: 10.1007/s11207-022-02073-7

Press, W. H., Teukolsky, S. A., Vetterling, W. T., & Flannery, B. P. 1992, Numerical recipes in FORTRAN. The art of scientific computing

Reiner, M. J., Kaiser, M. L., & Bougeret, J. L. 2007, *ApJ*, 663, 1369, doi: 10.1086/518683

Syed Ibrahim, M., Joshi, B., Cho, K. S., Kim, R. S., & Moon, Y. J. 2019, *SoPh*, 294, 54, doi: 10.1007/s11207-019-1443-5